Nanotechnology **22** (2011) 135302 (8pp) doi:10.1088/0957-4484/22/13/135302

Wettability control by DLC coated nanowire topography

Zihui Li[1,2], **Fanhao Meng**[1] **and Xuanyong Liu**[1,3]

[1] State Key Laboratory of High Performance Ceramics and Superfine Microstructure, Shanghai Institute of Ceramics, Chinese Academy of Sciences, 1295 Dingxi Road, Shanghai 200050, People's Republic of China
[2] Graduate School of Chinese Academy of Sciences, Shanghai 200050, People's Republic of China

E-mail: xyliu@mail.sic.ac.cn

Received 29 November 2010, in final form 18 January 2011
Published 22 February 2011
Online at stacks.iop.org/Nano/22/135302

Abstract
Here we have developed a convenient method to fabricate wettability controllable surfaces that can be applied to various nanostructured surfaces with complex shapes for different industrial needs. Diamond-like carbon (DLC) films were synthesized on titanium substrate with a nanowire structured surface using plasma immersion ion implantation and deposition (PIII&D). The nanostructure of the DLC films was characterized by field emission scanning electron microscopy and found to grow in a rippling layer-by-layer manner. Raman spectroscopy was used to investigate the different bonding presented in the DLC films. To determine the wettability of the samples, water contact angles were measured and found to vary in the range of 50°–141°. The results indicated that it was critical to construct a proper surface topography for high hydrophobicity, while suitable I_D/I_G and sp^2/sp^3 ratios of the DLC films had a minor contribution. Superhydrophobicity could be achieved by further CF_4 implantation on suitably structured DLC films and was attributed to the existence of fluorine. In order to maintain the nanostructure during CF_4 implantation, it was favorable to pre-deposit an appropriate carbon content on the nanostructure, as a nanostructure with low carbon content would be deformed during CF_4 implantation due to local accumulation of surface charge and the following discharge resulting from the low conductivity.

1. Introduction

Wettability is one of the most important surface properties of materials, especially when the materials are used for self-cleaning [1], water–oil separation [2], no-loss transport of microdroplets [3], and biomedical applications such as blood-contacting medical devices [4, 5] and cell-contacting hard tissue implants [6, 7]. Wettability can be characterized by measuring the contact angle of a static water droplet on the material surface. Usually a surface with a contact angle less than 90° is defined as hydrophilic, while one with a contact angle greater than 90° is defined as hydrophobic. Wettability of material is mainly dominated by its surface topography and chemical composition, and can be modified by altering these two dominant factors. In recent years, high hydrophobic surfaces, especially superhydrophobic surfaces with water contact angle greater than 150°, have gained much attention for both fundamental research and practical applications [8]. Inspired by the 'lotus effect', a fascinating phenomenon in Nature which has the attractive ability of self-cleaning, researchers concluded that there were mainly two ways to obtain high hydrophobic surfaces: by constructing a proper nanostructure on a hydrophobic surface, or by coating a nanostructure surface with a layer of low surface energy material [9, 10]. Titanium is widely used in the fields of the aerospace industry, the chemical industry, machinery and medical devices. Tailoring the wettability of titanium by surface treatment has both theoretical and practical importance, as wettability is closely related to other surface properties, such as photocatalytic activity [11], adhesive bonding [12], blood compatibility [13] and cell function [14]. Researches have indicated that titanium based implants with a hydrophobic

[3] Author to whom any correspondence should be addressed.

surface would strongly affect the initial interaction with the physiological environment, including the adhesion of some specific proteins [15, 16], behavior regulation of different cells [17–19], etc, which might enable us to tailor the biological responses to titanium surface according to different clinical needs.

Diamond-like carbon (DLC) is an effective material to modify the surface wettability by lowering the surface energy and altering the surface topography [20–22]. DLC films can be constructed onto smooth surfaces as well as various nanostructured surfaces, such as ablation aluminum substrate and electroplating copper foil [23], via many available techniques such as chemical vapor deposition (CVD) [20], electrodeposition [22], cathodic micro-arc discharge [24], and magnetron sputtering [21]. The combination of the structural variability of carbon and the controlled structured surface will surely extend the application of the wettability alterable carbon thin films, as wettability and surface structure are both considered as important factors for materials.

Plasma immersion ion implantation and deposition (PIII&D) is one of the surface modification technologies which has been frequently used to prepare surface coatings in the last few decades. PIII&D is suitable for modifying large-scale surface and multifaceted devices with complex 3D shapes due to its non-line-of-sight nature, which makes it superior to the line-of-sight methods such as conventional beam-line ion implantation and CVD. Carbon thin films synthesized by PIII&D have attracted much attention in recent years and were reported to have potential applications as biomedical materials [6, 25–27], precision bearing materials in the aerospace industry [28], and other materials which required superior hardness, corrosion resistance and wear resistance. However, as far as we know, modification of the surface wettability by fabricating DLC films on nanostructured surface using PIII&D has not been explored, even though the PIII&D technique is a convenient method for depositing surface coatings and tailoring the surface topography.

The objective of this work was to modify the surface topography and hence the surface wettability by combining DLC films with a nanostructured surface. DLC films were synthesized on a titanium surface with a nanowire structure by PIII&D at various experimental conditions using acetylene as a carbon precursor. CF_4 implantation was further conducted to achieve superhydrophobicity. The changes in surface topography, chemistry and thereby on wettability of the DLC films were studied, which provided an opportunity to understand the relationship between wettability and surface character of the material. Herein, we develop a feasible method for the fabrication of wettability controllable DLC films coated on nanostructured surfaces.

2. Experimental details

2.1. Materials preparation

Commercial pure Ti plates with dimensions of 10 mm × 10 mm × 1 mm were ultrasonically cleaned in ethanol and deionized water several times, followed by pickling in a 5 wt% oxalic acid solution at 100 °C for 2 h to remove the oxide layer and obtain a homogeneous rough surface [29]. Then the samples were ultrasonically cleaned in deionized water and dried in ambient atmosphere for further use. The TiO_2 nanowire structure on the Ti surface was prepared according to the literature [29]. Briefly, each pretreated Ti plate was immersed in a mixed solution of 5 ml H_2O_2 (30 wt%) and 5 ml NaOH (5 M) in a reaction vessel with Teflon liner at 80 °C for 24 h. After the reaction vessel cooled to room temperature, the Ti plates were gently rinsed with deionized water and protonated in 0.1 M HCl for 2 h. Then the Ti plates were rinsed to neutral with deionized water, dried in ambient atmosphere, and finally calcined at 450 °C for 1 h. Ti substrates with nanowire structured surfaces were obtained and denoted as NT.

Table 1. C_2H_2 deposition parameters.

Sample	DC bias voltage (V)	Deposition time (min)
I-NT	0	0
I&D-1	0	5
I&D-2	20	5
I&D-3	40	5
I&D-4	40	10

A series of DLC films were prepared on the surface of as-prepared NT by PIII&D using acetylene (C_2H_2) as a carbon precursor. The background pressure of the plasma chamber was evacuated to 5×10^{-3} Pa before the experiment. A C_2H_2 flow of 50 standard cubic centimeters per minute (sccm) was introduced into the chamber under an implantation voltage of 15 kV during the 5 min implantation procedure. The pulse frequency and pulse duration were 70 Hz and 50 μs, respectively. The working pressure was about 10^{-1} Pa. The samples which were only conducted by the implantation process were denoted as I-NT. During the following deposition procedure, a 50 sccm C_2H_2 flow was introduced into the chamber and the plasma was triggered using a radio frequency power of 300 W with pulse bias voltage of 550 V. The samples which were treated by the deposition procedure with different direct current (DC) bias voltages and deposition times were denoted as I&D-x (x = 1–4), as listed in table 1. Then the as-prepared NT and the DLC films on nanowire structured Ti substrates were treated by tetrafluoromethane (CF_4) implantation. The CF_4 flow was 50 sccm, the implantation voltage was 15 kV and the pulse duration was 50 μs. The pulse frequency was set as 50 Hz in order to maintain the surface nanostructure.

2.2. Surface characterization

The surface morphologies and chemical compositions of the samples were characterized by field emission scanning electron microscopy (FE-SEM; S-4800, HITACHI, Japan) and Auger electron spectroscopy with x-ray photoelectron spectrum (AES with XPS; Microlab 310-F Scanning Auger Microprobe with a dual anode (Al/Mg) x-ray source). An accelerating voltage of 10 kV was used in the FE-SEM analysis. An Al Kα (1486.6 eV) source was used in the XPS analysis. Raman spectroscopy was used to investigate the

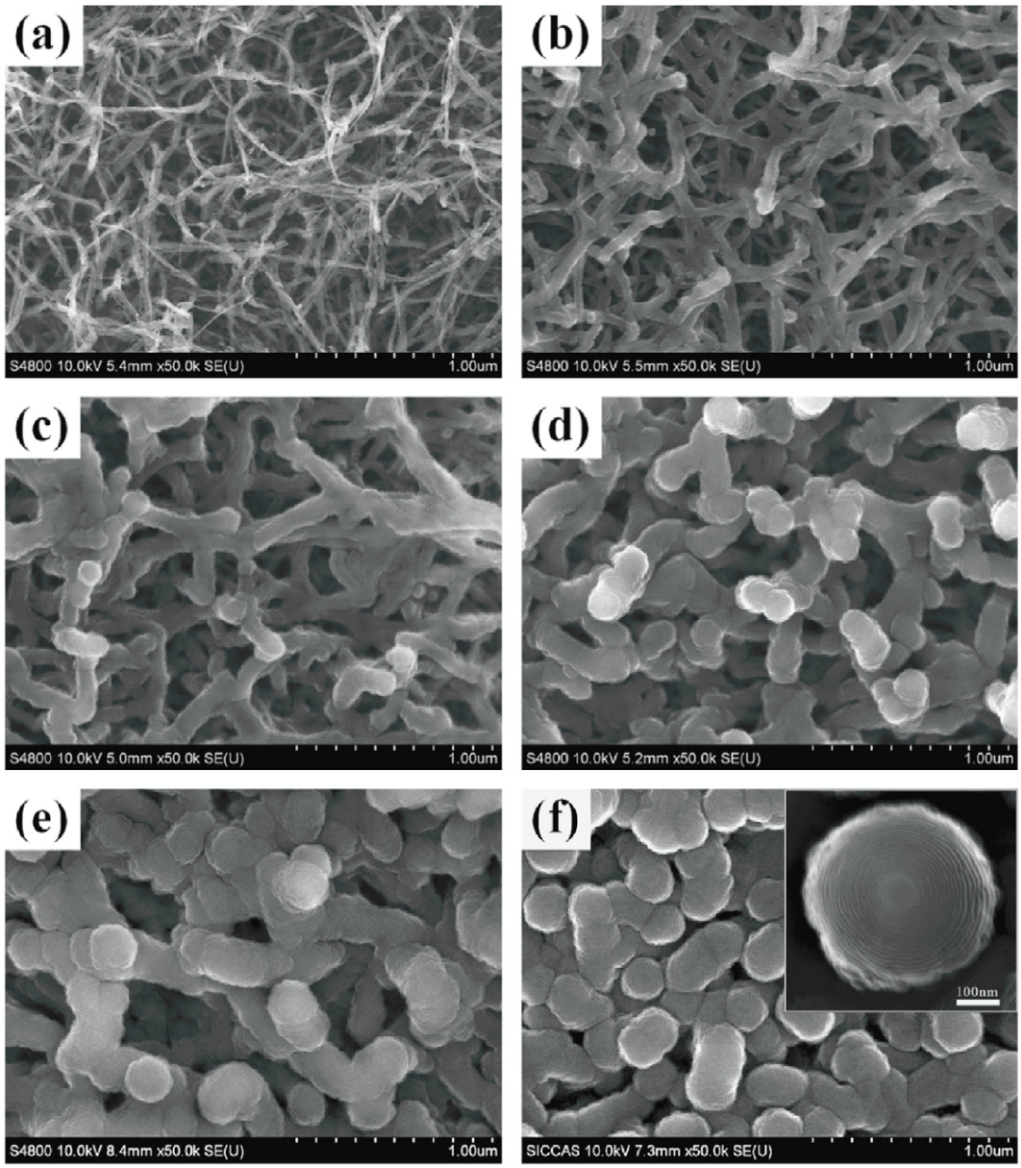

Figure 1. Surface views of various samples: (a) NT, (b) I-NT, (c) I&D-1, (d) I&D-2, (e) I&D-3 and (f) I&D-4, the inset is a higher magnification of the layered spherical carbon structure of I&D-4.

different bondings presented in the samples using a Raman microscope system (Horiba Jobin Yvon HR800, France) with an Ar-ion laser at 20 mW (514.5 nm) for excitation. The surface wettability of the samples was measured by contact angle measurement (Automatic Contact Angle Meter Model SL200B, Solon (Shanghai) information technology Co., Ltd, China), conducted in ambient environment using 2 μl sessile distilled water droplets.

3. Results and discussion

Figure 1 shows the surface photographs of NT, I-NT, I&D-1, I&D-2, I&D-3 and I&D-4 respectively. The porous NT surface contained numerous nanowires with diameters of 30–40 nm, which entangled with each other and formed a network (figure 1(a)). After treatment by C_2H_2 plasma immersion ion implantation, the as-prepared interconnected nanowires were coated with a thin layer of carbon films (figure 1(b)). The diameter of the nanowires was increased to about 80 nm and the nanowire network was well maintained. Figure 1(c) depicts the surface topography of I&D-1, where the deposition step was conducted with a pulse bias voltage of 550 V and a direct current bias voltage of 0 V for 5 min. The amount of carbon obtained in the deposition step was governed by the direct current bias voltage. The deposition rate was relatively low without direct current bias voltage and the diameter of the obtained nanowires was about 130 nm (figure 1(c)). The diameter of the nanowires continued to grow larger to 170–180 nm with the direct current bias voltage increasing to 20 V (figure 1(d)). The bottom of the porous structure was partially filled with deposited carbon. When the direct current bias voltage was increased to 40 V, part of the porous surface was connected by deposited carbon films while some remained as porous nanowire structure (figure 1(e)). By extending

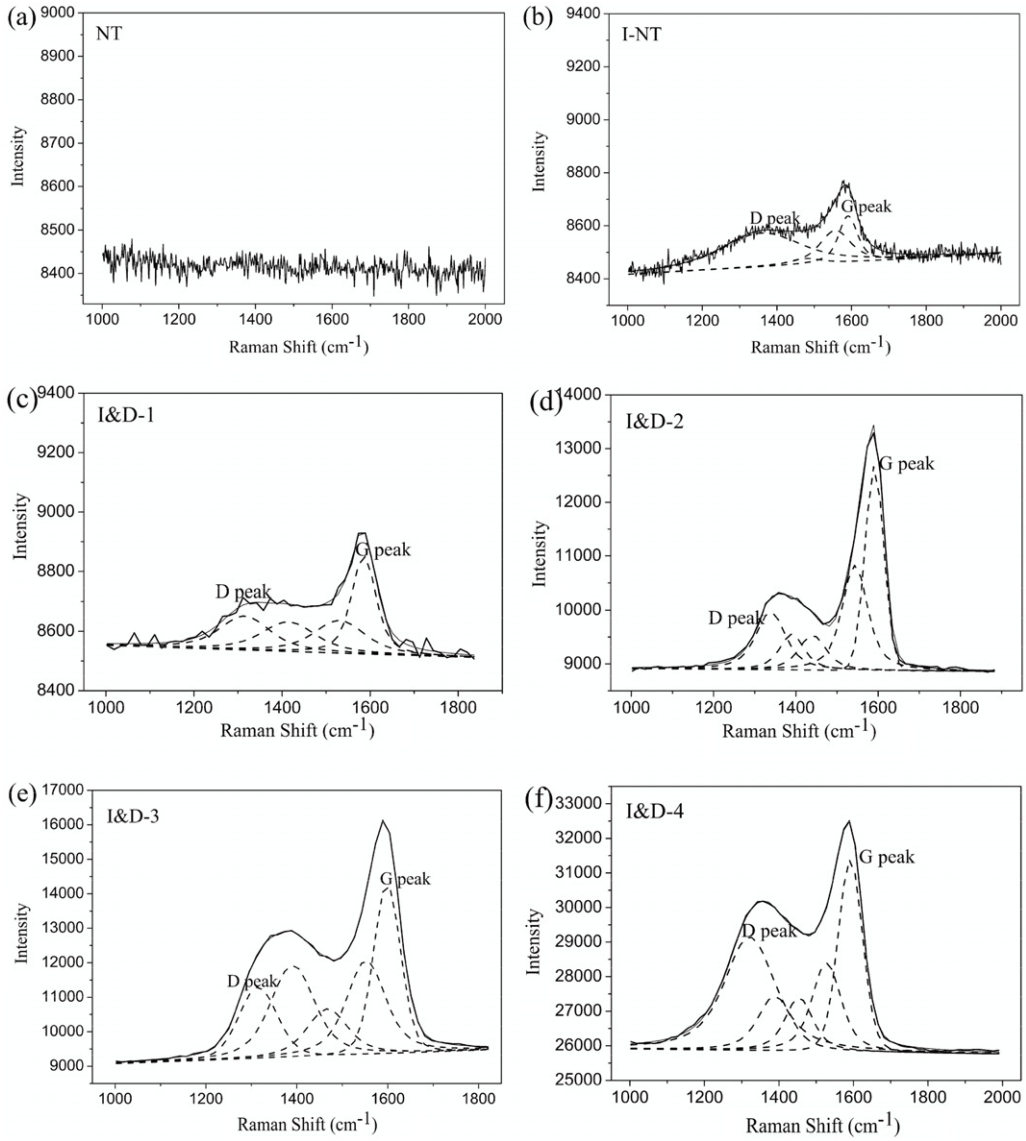

Figure 2. Raman spectra of the as-prepared nanowire structured Ti (NT) (a) and the synthesized DLC films: (b) I-NT, (c) I&D-1, (d) I&D-2, (c) I&D-3 and (c) I&D-4.

the deposition time from 5 to 10 min under a direct current bias voltage of 40 V, the porous nanowire network almost disappeared and the surface was covered by continuous carbon films (figure 1(f)).

Interestingly, we found that the DLC films coated on the nanowire structured surface synthesized by PIII&D grew in a layer-by-layer manner. When the films grew to a certain extent and exceeded the top of the nanowire, a layered spherical structure appeared (figures 1(d)–(f)). A higher magnification of the layered spherical carbon in figure 1(f) is displayed in the inset. It has been reported that carbon films with spherical structures were synthesized using CVD methods [20, 30]. However, the subtle structure of the sphere has not been reported. The formation of this rippling layered structure may be partially attributed to the growth mode of nucleation and deposition in gas atmosphere [20]. The nature of carbon was another important factor for the layer-by-layer manner. The properties of the DLC films were actually more similar to those of graphite, which has a layered structure.

Raman spectra of the as-prepared nanowire structured Ti (NT) and the synthesized DLC films are shown in figure 2, the order of which corresponds to the sequence of the surface photographs in figure 1. There was no peak between the Raman shifts at 1000 and 2000 cm^{-1} in figure 2(a), indicating that NT did not cause Raman scattering in this area. The Raman spectra in figures 2(b)–(f) were deconvoluted into several peaks using a multiple Lorentzian peak fit. The presence of typical D and G peaks at around 1340 cm^{-1} and 1590 cm^{-1}, respectively, confirmed the formation of DLC films. The G peak is a measure of all sp^2 sites while the D peak is only due to the six-fold ring structure in the DLC films [31]. The ratio of the intensity of the D peak to the intensity of the G peak (I_D/I_G) as well as the relative presence of sp^2 and sp^3 bonds (sp^2/sp^3) were evaluated and are shown in figure 3. Figure 3(a)

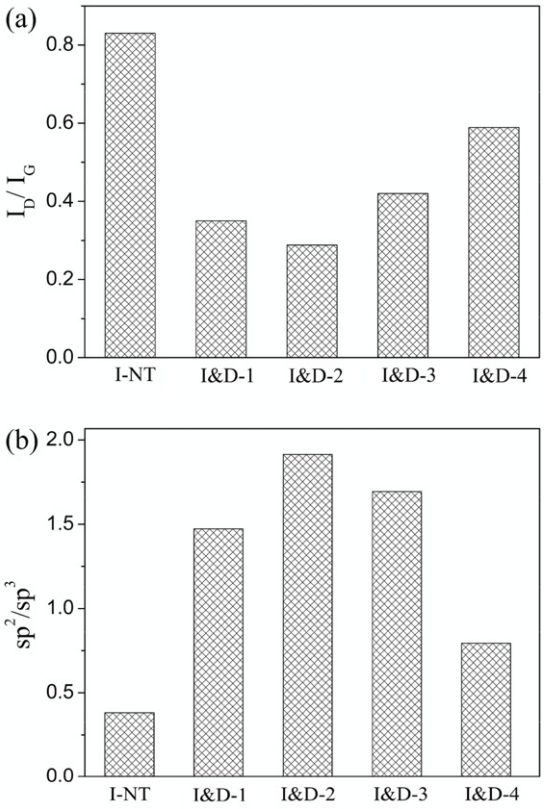

Figure 3. I_D/I_G ratio (a) and sp^2/sp^3 ratio (b) of the synthesized DLC films.

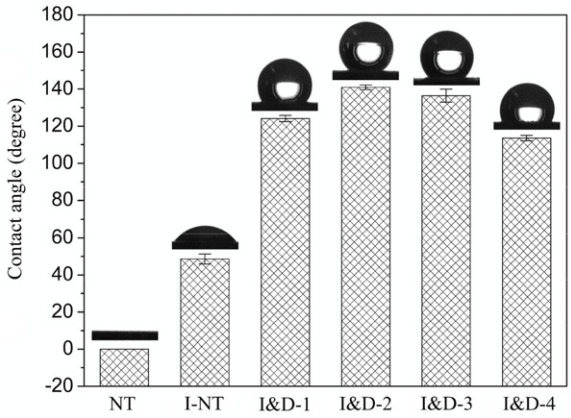

Figure 4. Contact angle of NT and the synthesized DLC films.

indicates that the synthesized DLC films had a lower I_D/I_G ratio after the deposit step. I&D-2 had the lowest I_D/I_G ratio, followed by I&D-1, I&D-3 and I&D-4 sequentially, while I-NT had the highest I_D/I_G ratio. It was reported that the relative intensity of the D and G peaks increased with substrate temperature [32]. The ion bombardment as well as the surface charge accumulation due to the low conductive surface in the implantation step caused thermal accumulation on the surface of I-NT, which contributed to the highest I_D/I_G ratio. However, the temperature rise in the deposition step would be relatively lower. The high I_D/I_G ratio of I&D-4 was attributed to the thermal accumulation due to the prolonged deposition time. From figure 3(b) we can see that the sp^2/sp^3 ratio increased rapidly from I-NT to I&D-1, reached the highest level in I&D-2, and then decreased gradually in I&D-3 and I&D-4. The sp^2/sp^3 ratio in DLC films depended on experimental conditions such as substrate deposition temperature [33], type and pressure of the precursor gas [34]. In the present study, a possible reason for the change of sp^2/sp^3 ratio might be that as the DC bias voltage increased in the deposition step, the particle bombardment function was enhanced and the sp^3-bond carbon density was reduced [35].

The water contact angles of NT and the synthesized DLC films are displayed in figure 4. They represented the wettability of the surfaces and mainly depended on the surface topography. The as-prepared nanowire structured surface was superhydrophilic with a contact angle of 0°, indicating that the water droplets would spread rapidly when they made contact with the surface. The hydrophilic property of TiO_2 [36] was magnified by the porous nanowire structure and became superhydrophilic, because it is much easier for water to penetrate into the surface layer. The contact angle of I-NT was close to 50°, mainly due to the hydrophobicity of DLC films. But the surface remained hydrophilic because the pores among the nanowires were still large enough for the water droplet to penetrate. After the deposition step was conducted the samples all exhibited hydrophobic behavior with the contact angle varying between 112° and 141°. The largest contact angle, about 141°, appeared on the surface of I&D-2. It was a result of the appropriate nanostructure with suitable pore size and porosity. The contact angle hysteresis of I&D-2 was very high. The water droplet on its surface could not roll off even when the sample was tilted vertically, while it still appeared spherical in shape. Those samples with oversize pores (I&D-1) and too small a porosity (I&D-3) were less hydrophobic. The surface of I&D-4 was covered up by DLC films and the primary nanowire structure was hardly found, resulting in a contact angle of around 112°.

In general, the surface topography, porosity and roughness are major factors for wettability [10, 20, 37]. A nanostructured surface should have the ability to form a large amount of entrapped air pockets so as to achieve high hydrophobicity, as air is an effective hydrophobic media [38]. When water was dropped onto the nanowire structured surface coated with DLC films, air was entrapped in the pores to form air pockets and the liquid–air contact area was enlarged. However, the entrapped air pockets were unstable and could easily collapse if the pores on the surface were too large. The reason why I-NT was still hydrophilic might be the overlarge pore size. From figure 1(b) we can see that the original interconnected nanowire network was well maintained despite the nanowire being coated with a thin layer of DLC films. Water could still penetrate into the large pores when the droplet was connected with the surface. To achieve a high hydrophobic surface, the topography of the surface was tailored by altering the PIII&D parameters. The surface of I&D-1 was more suitable for the formation of stable air pockets and hence more hydrophobic, because the pore size of the surface layer was smaller while the diameter of the DLC coated nanowire was enlarged (figure 1(c)). The most hydrophobic I&D-2 was considered to have a proper surface topography with suitable pore size and porosity and

hence could form a high fraction of liquid–air contact area when contacting with a water droplet (figure 1(d)). On the other hand, ultrasmall pore size and porosity could result in less hydrophobicity because of the limited amount of air pockets. When the DLC films became thicker the pore size and porosity were smaller accordingly, which made I&D-3 less hydrophobic than I&D-2 (figure 1(e)). Figure 1(f) shows that the surface of I&D-4 was relatively flat with a few small pores, which led to its lowest hydrophobicity among the samples from implantation and deposition. So it was critical to form a surface topography with suitable pore size and porosity for high hydrophobicity.

The Cassie–Baxter equation, $\cos\theta_r = f_1 \cos\theta - f_2$, could be used to explain the high hydrophobicity of I&D-2 [39–41]. Here θ_r (141°) and θ (51°) were the contact angles of I&D-2 and the smooth titanium surface coated with DLC films under the same experimental conditions, respectively; f_1 and f_2 were the contact area fractions of liquid–solid and liquid–air, respectively ($f_1 + f_2 = 1$). According to the equation, the value of f_1 was 0.14, which indicated that only 14% of the total liquid-contacting area was liquid–solid contact, whereas the other 86% of the area was liquid–air contact. As a result, the water droplet appeared as a spherical shape to minimize its liquid–air interfacial energy.

On the other hand, chemical bonding and surface passivation also had impact on the surface wetting behavior, but with less influence than the previous factors [20]. There were two minor factors here which should be taken into account besides the crucial factor: the I_D/I_G and sp^2/sp^3 ratios. It was reported that the contact angle decreased rapidly with increasing I_D/I_G ratio, which measured the fraction of the ring organized sp^2 phase [22]. In the present study, I-NT had the lowest contact angle and the highest I_D/I_G ratio. There was a decrease of the I_D/I_G ratio from I&D-1 and I&D-2 and the contact angle increased sharply. Then the I_D/I_G ratio increased and hence the contact angle became lower again, which corresponded with the previous research [22]. Some researchers indicated that the increasing sp^2 content in the carbon film caused a reduction of surface free energy and hence enhanced the hydrophobicity [20, 42, 43]. From figures 3(b) and 4 we can see that the sequence of sp^2/sp^3 ratio corresponds well with the wetting behavior, which confirms the previous rule. The highest sp^2/sp^3 ratio of I&D-2 was attributed partially to its high hydrophobicity, while the hydrophilic I-NT had the lowest sp^2/sp^3 ratio. However, the DLC films could not achieve a contact angle as high as 141° merely by modifying the I_D/I_G and sp^2/sp^3 ratios. Control experiments showed that the contact angle of DLC films synthesized on smooth Ti surfaces without nanowire structure using PIII&D varied between 33° and 60°. Generally speaking, the surface topography was playing a leading role in making I&D-2 the most hydrophobic sample, while the properties of the DLC films had a relatively minor contribution.

CF_4 implantation had different effects on the series of nanowire structures with or without DLC films. It was reported that the existence of fluorine would remarkably reduce the surface energy and enhance hydrophobicity [21]. However, in the present study we found that CF_4 implantation did not always cause an increase in contact angle. NT remained superhydrophilic and, unexpectedly, the contact angle of I-NT decreased from around 50° to 0° after CF_4 implantation. I&D-1, I&D-2, I&D-3 and I&D-4 exhibited much larger contact angles after CF_4 implantation, varying between 132° and 150°. I&D-2 became superhydrophobic with a contact angle of 150° after CF_4 implantation. Figure 5 depicts the surface topography of CF_4 implanted I-NT and I&D-2 and the insets show the shapes of the water droplets on the corresponding surfaces. The surface topography of the samples revealed the reason why CF_4 implantation caused converse change on the wettability of I-NT and other samples. From figure 5(a) we can see that CF_4 implantation caused deformation of the nanowire structure on the I-NT surface, resulting in a random porous surface through which water could penetrate easily. The reason may be that the conductivity of the I-NT surface was fairly low due to the relatively low carbon content. During CF_4 implantation, the low conductive surface caused local accumulation of surface charge, and the following surface discharge destroyed the nanostructure. However, the nanowire structure on the surface of I&D-2 was quite well maintained after CF_4 implantation, mainly due to the good conductivity of the DLC films (figure 5(b)). The surface topography of the DLC films on CF_4 implanted I&D-2 was slightly different from that before CF_4 implantation, mainly due to the low carbon content in the CF_4 plasma.

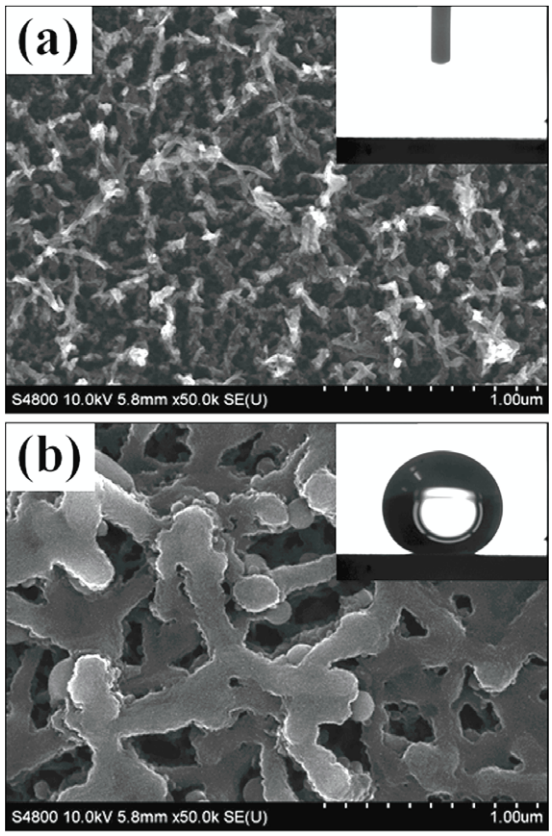

Figure 5. Surface topography of CF_4 implanted I-NT (a) and I&D-2 (b), the insets show the shapes of the water droplets on the corresponding surfaces.

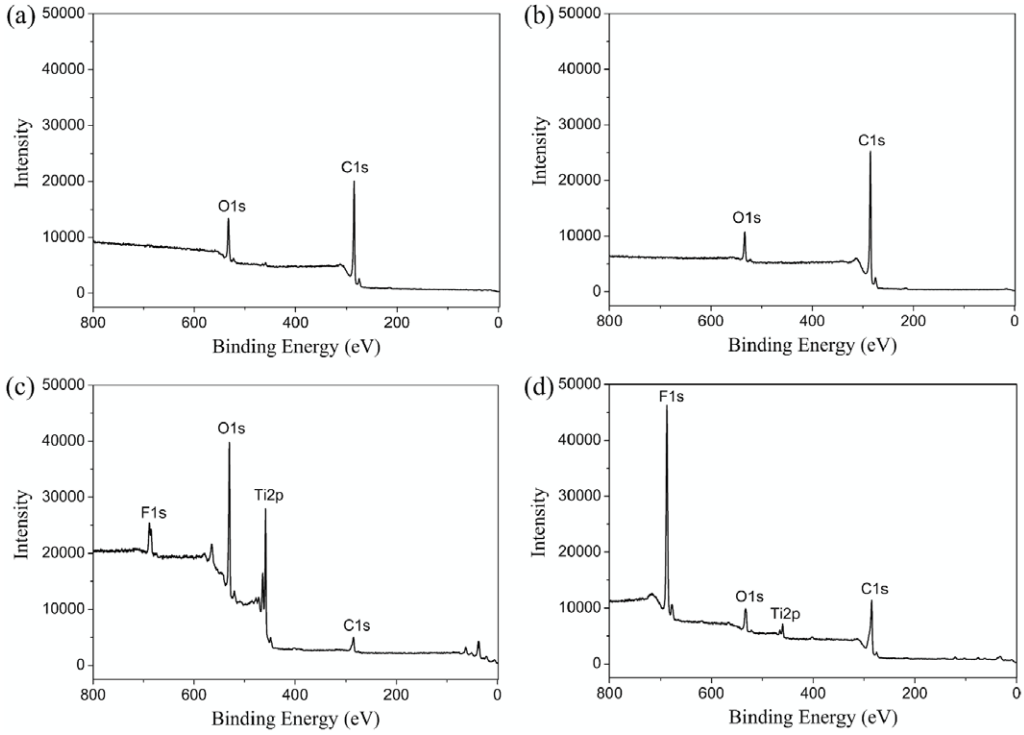

Figure 6. XPS full spectra of various samples: (a) I-NT, (b) I&D-2, (c) CF_4 implanted I-NT and (d) CF_4 implanted I&D-2.

CF_4 molecules were reported to be decomposed easily to various radicals in the plasma [21]. During CF_4 implantation, the unsaturated C bonds of the DLC films were saturated by the CF_x bonds during the plasma treatment and the hydrophobicity of the DLC films was enhanced. However, a control experiment showed that the contact angle of CF_4 implanted DLC films synthesized on smooth Ti surface varied between 45° and 76°, indicating that the CF_x bonds alone could not lead to superhydrophobicity. Figure 6 shows the XPS full spectrum of I-NT and I&D-2 before and after CF_4 implantation, respectively. The carbon content of I&D-2 was obviously higher than that of I-NT, which was confirmed previously by their surface views (figures 1(b) and (d)) and Raman spectra (figures 2(b) and (d)). The fluorine content of CF_4 implanted I&D-2 (figure 6(d)) was much higher than that of CF_4 implanted I-NT (figure 6(c)), indicating that higher carbon content would facilitate the bonding between DLC films and CF_x, as there were more unsaturated C bonds on the outermost surface. On the other hand, figures 6(c) and (d) reveal the different extents of surface deformation. The surface nanostructure of CF_4 implanted I-NT was destroyed to a large extent and the deformed TiO_2 nanowire structure was exposed on the surface, resulting in a relatively high Ti content in figure 6(c). The bonding of fluorine to TiO_2 was weaker than to carbon, which also attributed to the lower fluorine content on the surface of CF_4 implanted I-NT. Figure 6(d) shows that only a small amount of TiO_2 was detected on the surface of CF_4 implanted I&D-2, indicating that the damage of the surface caused by CF_4 implantation was limited and hence the content of CF_x bonding on the surface DLC films was greatly increased. The superhydrophobicity of CF_4 implanted I&D-2 was attributed to the suitable surface topography as well as the existence of fluorine in the DLC films.

4. Conclusions

The wettability of titanium was controlled by synthesizing DLC films on its nanowire structured surface using PIII&D technology in this work. The DLC films on the nanowire structured titanium surface grow in a layer-by-layer manner into a spherical structure. The high hydrophobicity of the nanowire structured titanium with DLC films is attributed to the proper nanostructure topography with suitable pore size and porosity, while a lower I_D/I_G ratio and a higher sp^2/sp^3 ratio of the DLC films also have a relatively minor contribution. Further CF_4 implantation on suitably structured DLC films can lead to superhydrophobicity. This study provides a convenient method to control the wettability of substrates with complex shapes from hydrophilic to superhydrophobic according to practical needs.

Acknowledgments

This work was jointly supported by Shanghai-Unilever Research and Development Fund 09520715200, Shanghai Science and Technology R&D Fund under grants 0952nm04400 and 1052nm06600, National Natural Science Foundation of China No. 51071168, Innovation Fund of SICCAS under grant Y06ZC3130G.

References

[1] Jin M H, Feng X J, Xi J M, Zhai J, Cho K W, Feng L and Jiang L 2005 *Macromol. Rapid Commun.* **26** 1805–9
[2] Wang S T, Song Y L and Jiang L 2007 *Nanotechnology* **18** 015103
[3] Cheng Z J, Feng L and Jiang L 2008 *Adv. Funct. Mater.* **18** 3219–25
[4] Sun T L, Tan H, Han D, Fu Q and Jiang L 2005 *Small* **1** 959–63
[5] Yang P, Huang N, Leng Y X, Chen J Y, Wang J, Sun H, Wan G J and Zhao A S 2010 *Surf. Coat. Technol.* **204** 3039–42
[6] Chai F, Mathis N, Blanchemain N, Meunier C and Hildebrand H F 2008 *Acta Biomater.* **4** 1369–81
[7] Stancu E C, Ionita M D, Vizireanu S, Stanciuc A M, Moldovan L and Dinescu G 2010 *Mater. Sci. Eng.* B **169** 119–22
[8] Feng L, Li S H, Li Y S, Li H J, Zhang L J, Zhai J, Song Y L, Liu B Q, Jiang L and Zhu D B 2002 *Adv. Mater.* **14** 1857–60
[9] Sun T L, Feng L, Gao X F and Jiang L 2005 *Acc. Chem. Res.* **38** 644–52
[10] Barthlott W and Neinhuis C 1997 *Planta* **202** 1–8
[11] Guan K H 2005 *Surf. Coat. Technol.* **191** 155–60
[12] Leahy W, Barron V, Buggy M, Young T, Mas A, Schue F, McCabe T and Bridge M 2001 *J. Adhes.* **77** 215–49
[13] Tsyganov I, Maitz M F, Wieser E, Richter E and Reuther H 2005 *Surf. Coat. Technol.* **200** 1041–4
[14] Tsukimura N, Kojima N, Kubo K, Att W, Takeuchi K, Kameyama Y, Maeda H and Ogawa T 2008 *J. Biomed. Mater. Res.* A **84A** 108–16
[15] Muller C, Luders A, Hoth-Hannig W, Hannig M and Ziegler C 2010 *Langmuir* **26** 4136–41
[16] Rupp F, Scheideler L, Rehbein D, Axmann D and Gels-Gerstorfer J 2004 *Biomaterials* **25** 1429–38
[17] Lai H C, Zhuang L F, Liu X, Wieland M, Zhang Z Y and Zhang Z Y 2010 *J. Biomed. Mater. Res.* A **93A** 289–96
[18] Rausch-fan X H, Qu Z, Wieland M, Matejka M and Schedle A 2008 *Dent. Mater.* **24** 102–10
[19] Eriksson C, Nygren H and Ohlson K 2004 *Biomaterials* **25** 4759–66
[20] Banerjee D, Mukherjee S and Chattopadhyay K K 2010 *Carbon* **48** 1025–31
[21] Zhou Y, Wang B, Zhang X H, Zhao M, Li E and Yan H 2009 *Colloids Surf.* A **335** 128–32
[22] Paul R, Dalui S, Das S N, Bhar R and Pal A K 2008 *Appl. Surf. Sci.* **255** 1705–11
[23] Schulz H, Leonhardt M, Scheibe H J and Schultrich B 2005 *Surf. Coat. Technol.* **200** 1123–6
[24] Kong X H, Wang S A, Zhao H P and He Y D 2010 *Thin Solid Films* **518** 4211–4
[25] Poon R W Y, Yeung K W K, Liu X Y, Chu P K, Chung C Y, Lu W W, Cheung K M C and Chan D 2005 *Biomaterials* **26** 2265–72
[26] Wang J, Huang N, Yang P, Leng Y, Sun H, Liu Z Y and Chu P K 2004 *Biomaterials* **25** 3163–70
[27] Yang P, Huang N, Leng Y X, Chen J Y, Fu R K Y, Kwok S C H, Leng Y and Chu P K 2003 *Biomaterials* **24** 2821–9
[28] Zeng Z M, Zhang T, Tian X B, Tang B Y, Kwok T K and Chu P K 2000 *Surf. Coat. Technol.* **128** 236–9
[29] Wu Y H, Long M C, Cai W M, Dai S D, Chen C, Wu D Y and Bai J 2009 *Nanotechnology* **20** 185703
[30] Yan A H, Xiao X C, Kulaots I, Sheldon B W and Hurt R H 2006 *Carbon* **44** 3116–20
[31] Robertson J 2002 *Mater. Sci. Eng.* R **37** 129–281
[32] Fuge G M, May P W, Rosser K N, Pearce S R J and Ashfold M N R 2004 *Diamond Relat. Mater.* **13** 1442–8
[33] Balon F, Stolojan V, Silva S R P, Michalka M and Kromka A 2005 *Vacuum* **80** 163–7
[34] Ossi P M, Bottani C E and Miotello A 2005 *Thin Solid Films* **482** 2–8
[35] Wang J, Liu G C, Wang L D, Deng X L and Xu J 2008 *Chin. Phys.* B **17** 3108–14
[36] Hashimoto K, Irie H and Fujishima A 2005 *Japan. J. Appl. Phys.* Part 1 **44** 8269–85
[37] Gao X F and Jiang L 2004 *Nature* **432** 36
[38] Lai Y, Gao X, Zhuang H, Huang J, Lin C and Jiang L 2009 *Adv. Mater.* **21** 3799–803
[39] Cassie A B D and Baxter S 1944 *Trans. Faraday Soc.* **40** 0546–50
[40] McHale G 2007 *Langmuir* **23** 8200–5
[41] Pan Q M, Jin H Z and Wang H 2007 *Nanotechnology* **18** 355605
[42] Zhou Y, Wang B, Song X, Li E, Li G, Zhao S and Yan H 2006 *Appl. Surf. Sci.* **253** 2690–4
[43] Yan X B, Xu T, Yue S S, Liu H W, Xue Q J and Yang S R 2005 *Diamond Relat. Mater.* **14** 1342–7